Brain network mechanisms of visual shape completion

Brian P. Keane [1,2], Deanna M. Barch[3], Ravi Mill[4], Steven M. Silverstein [1,2,5], Bart Krekelberg [4*], Michael W. Cole [4*]

[1] University Behavioral Health Care, Department of Psychiatry, and Center for Cognitive Science, Rutgers, The State University of New Jersey

[2] Departments of Psychiatry and Neuroscience, University of Rochester Medical Center

[3] Departments of Psychological & Brain Sciences, Psychiatry, and Radiology, Washington University in St. Louis

[4] Center for Molecular and Behavioral Neuroscience, Rutgers, The State University of New Jersey

[5] Department of Ophthalmology, University of Rochester Medical Center

* Co-senior authors

Number of pages: 39

Number of figures: 6

Number of tables: 1

Number of words, Abstract: 250

Number of words, Introduction: 603

Number of words, Discussion: 1605

Acknowledgments: This work was supported by a National Institutes of Health Mentored Career Development Award (K01MH108783) to BPK. We thank Laura Crespo, Lisa Cruz, Dillon Smith, and Megan Serody for help in recruiting participants and collecting and organizing study data. We are also indebted to Michael Harms for assistance in finalizing the pulse sequence, and Takuya Ito and Carrisa Cocuzza for providing sample code. The authors additionally acknowledge the Office of Advanced Research Computing (OARC) at Rutgers University for providing access to the Amarel cluster and associated research computing resources (http://oarc.rutgers.edu).

Dedications: None.

Conflict of Interest: The authors declare no competing conflicts of interest.

Abstract

Visual shape completion recovers object size, shape, and position from sparsely segregated edge elements. Studies of the process have largely focused on occipital cortex, but the role of other cortical areas and their functional interconnections remains poorly understood. To reveal the functional networks, connections, and regions of shape completion across the entire cortex, we scanned (fMRI) healthy adults during rest and during a task in which they indicated whether four pac-men formed a fat or thin illusory shape (illusory condition) or whether non-shape-forming pac-men were uniformly rotated left or right (fragmented condition). Task activation differences (illusory-fragmented), resting-state functional connectivity, and multivariate pattern analyses were performed on the cortical surface using 360 predefined cortical parcels (Glasser et al., 2016) and 12 functional networks composed of such parcels (Ji et al., 2019). Brain activity flow mapping ("ActFlow") was used to evaluate the utility of resting-state connections for shape completion. Thirty-four parcels scattered across five functional networks were differentially active during shape completion. These regions were densely inter-connected during rest and a plurality occupied the secondary visual network. Posterior parietal, dorsolateral prefrontal, and orbitofrontal regions were also significant in the dorsal attention and frontoparietal networks. Functional connections from the dorsal attention network were key in modeling the emergence of activation differences (via ActFlow) in the secondary visual network and across all remaining networks. While shape completion is primarily driven by the secondary visual network, dorsal-attention regions are also involved, plausibly for relaying expectation-based signals about contour shape or position to ventral object-based areas.

Significance Statement: Visual shape completion is a fundamental process that combines scattered edge elements into unified representations of objects. The process has been extensively investigated in humans and animals, but neural studies have focused on lateral occipital and early visual regions with scant regard to given other parts of cortex or their functional interconnections. Here, we employed recent methods in network neuroscience and functional MRI to show that visual shape completion modulates a densely interconnected set of cortical regions; these primarily occupy the secondary visual network but may also be found in four other networks. Dorsal attention regions played a surprisingly prominent role in modeling activity within secondary visual network and across all remaining networks during shape completion.

Introduction

Visual shape completion recovers object shape, size, position, and numerosity from the relative alignments and orientations of spatially segregated edges. Converging evidence from human and non-human primates indicates that shape completion critically relies on V1, V2, V4, and lateral occipital cortex (LO), with feedback cascading from the latter two regions. For example, transcranial magnetic stimulation (TMS) applied earlier to LO (100-122 ms) or later over V1/V2 (160-182 ms) worsened discrimination of completed shapes (Wokke et al., 2013). In single-cell recordings, deep layer V2 cells responded ~100 ms post-stimulus onset and deep layer V1 cells responded at ~120-190 ms (Lee and Nguyen, 2001). Multielectrode array recordings of V4 revealed differential activity for completed shapes within ~150 ms and this was claimed to plausibly precede early visual activations (Cox et al., 2013 p.17099). Two photon calcium imaging in mouse has also shown that edge integration relies on long-range horizontal excitatory connections between V1 pyramidal cells (Iacaruso et al., 2017 p.451). These four regions—V1, V2, V4, and LO—have been termed the "classical" regions of shape completion (Keane, 2018) given their inter-connectedness and well-established role in the process.

To what extent do other regions participate in shape completion? At present, there is no consensus. Fusiform gyrus (Larsson et al., 1999a; Halgren et al., 2003) and V3B/KO have been implicated, although the latter has been found mainly, but not exclusively, with dynamic illusory contour stimuli (Kruggel et al., 2001). Monkey IT is more active during Kanizsa shape perception (see also, Huxlin et al., 2000; Sáry et al., 2008), however, this region is plausibly a human LO homologue (Orban et al., 2004). In one intriguing magnetoencephalography (MEG) study, adults passively viewed briefly presented pac-man stimuli (30 ms) with or without illusory contours; differential orbitofrontal cortex (OFC) occurred at 340 ms post stimulus onset (Halgren et al., 2003). The OFC effect has not been replicated perhaps because older fMRI studies had coarser spatial resolution, more partial voluming, and thus more signal drop-out near the sinuses (due to magnetic field inhomogeneities).

A problem is that many previous studies were conducted 10 to 20 years ago, with the last comprehensive review published in 2006 (Seghier and Vuilleumier, 2006). Earlier studies had fewer participants, less powerful magnets, larger voxel sizes (with partial voluming) and an inclination to focus on occipital cortex. Many were performed on expert psychophysical

observers or undergraduates (or both) and therefore were less likely to represent the general population (Henrich et al., 2010). Finally, and perhaps most critically, no work to our knowledge has examined the cortex-wide functional connections of shape completion.

Given these gaps in knowledge, our goal was to build upon foundational studies using more recent methods, a larger and more diverse participant sample, and an established shape completion task that has been described via psychophysics, fMRI, EEG, and TMS and that relies on the classical brain regions just mentioned (Gold et al., 2000; Pillow and Rubin, 2002; Murray et al., 2006; Keane et al., 2007; Wokke et al., 2013). We employed a multiband pulse sequence (with higher spatial/temporal resolution), a cortex-wide surface-based analysis (with better anatomical accuracy, Glasser et al., 2013), and a parcellation schema and network partition to dramatically reduce the number of statistical comparisons. We additionally used resting-state functional connectivity (RSFC) and brain activity flow mapping ("ActFlow") to assess the pathways that connect regions during shape completion. This last approach is justified since task and rest generate highly similar brain-wide functional connectivity (Cole et al., 2014; Krienen et al., 2014) and since integrating RSFC into ActFlow has yielded accurate predictions of the movement of task-evoked activations between brain regions (Cole et al., 2016).

Materials and Methods

Participants. The sample consisted of healthy controls who participated in a larger clinical study on the neural basis of abnormal visual perceptual organization in schizophrenia and bipolar disorder. These results are thus considered a first step in identifying how the brain represents—or fails to represent—visually completed shapes. The healthy sample comprised 20 psychophysically naïve participants (2 left handed, 8 females) with an average age of 37.6 and a racial composition of 35% African American, 10% Asian, 35% Caucasian, 15% mixed, and 5% unknown. A quarter of the participants were of Hispanic ethnicity. To obtain a more representative sample, we preferentially recruited controls without four-year college degrees, so that the average number of years of education was 14.8.

The inclusion/exclusion criteria were: (1) age 21-55; (2) no electroconvulsive therapy in the past 8 weeks; (3) no neurological or pervasive developmental disorders; (4) no drug dependence in the last three months (i.e., participants must not have satisfied more than one of the 11 Criterion A symptoms of DSM-5 substance use disorder in the last three months); (5) no

positive urine toxicology screen on the day of testing; (6) no brain injury due to accident or illness (e.g., stroke or brain tumor); (7) no amblyopia (as assessed by informal observation and self-report); (8) visual acuity of 20/32 or better (with corrective lenses if necessary); (9) the ability to understand English and provide written informed consent; (10) no scanner related contraindications (no claustrophobia, an ability to fit within the scanner bed, and no non-removable ferromagnetic material on or within the body); (11) no positive urine drug toxicology screen or breathalyzer test on the day of the scan; (12) no DSM-5 diagnosis of any psychotic or mood disorder; (13) no current psychotropic- or cognition-enhancing medication; (14) no first-degree relative with schizophrenia, schizoaffective, or bipolar disorder (as indicated by self-report).

Assessments. Psychiatric diagnosis exclusion was assessed with the Structured Clinical Interview for DSM-5 (SCID) (APA, 2000; First et al., 2002). Intellectual functioning of all subjects was assessed with a brief vocabulary test that correlates highly (r=0.80) with WAIS-III full-scale IQ scores (Shipley et al., 2009, p. 65; Canivez and Watkins, 2010). Visual acuity was measured with a logarithmic visual acuity chart under fluorescent overhead lighting (viewing distance = 2 meters, lower limit =20/10), and in-house visual acuity correction was used for individuals without appropriate glasses or contacts. Written informed consent was obtained from all subjects after explanation of the nature and possible consequences of participation. The study followed the tenets of the Declaration of Helsinki and was approved by the Rutgers Institutional Review Board. All participants received monetary compensation and were naive to the study's objectives.

Experimental Design and Statistical Analysis

Behavioral paradigm selection. Visual shape completion was investigated via a well-documented "fat/thin" discrimination paradigm in which subjects indicated whether an illusory Kanizsa square was fat or thin ("illusory" task) or whether four non-contour-forming pac-men were uniformly rotated left or right ("fragmented" task) (Ringach and Shapley, 1996). We define visual shape completion as the difference (in performance or activation) between the two task conditions. The fragmented task is a suitable control in that it requires judging the lateral rotational properties of the four pac-man, just like the illusory task. The two tasks also rely on a suite of common mechanisms for: (1) learning two response alternatives from a

limited number of practice exemplars and instructional screens (novel task learning); (2) transferring the learned alternatives to long term memory (consolidation); (3) attending to four discrete spatial regions (divided attention); (4) continuously monitoring the display over specific trial intervals (temporal attention); (5) capturing and extracting spatial information from briefly presented arrays (visual short term memory); (6) discerning fine-grained orientation differences (orientation perception); and (7) repeating the foregoing processes over the task duration (sustained motivation) (Keane et al., 2019). Perhaps because of these similarities, the two tasks are highly correlated behaviorally (Keane et al., 2019) and generate similar performance thresholds (Keane et al., 2014), which should not be taken for granted given that many visual tasks are uncorrelated (Grzeczkowski et al., 2017). In sum, by having employed a closely matched and already-tested control condition, we are in a position to identify mechanisms relatively unique to shape completion.

Stimulus and procedure. Subjects viewed the stimulus from a distance of 99 cm by way of a mirror attached to the head coil. There were four white sectored circles (radius = .88 deg, or 60 pixels) centered at the vertices of an invisible square (side = 5.3 deg, or 360 pixels), which itself was centered on a gray screen (RGB: 127; see Figure 3). Stimuli were initially generated with MATLAB and Psychtoolbox code (Pelli, 1997) with anti-aliasing applied for edge artifact removal. Images were subsequently presented in the scanner via PsychoPy (version 1.84; (Peirce, 2007) and a MacBook Pro laptop. Illusory contour formation depended on the geometric property of “relatability” (Kellman and Shipley, 1991): when the pac-men were properly aligned (relatable), the illusory contours were present (the “illusory” condition); when misaligned (unrelatable), they were absent (“fragmented” condition). A fixation point appeared at the screen center on each trial and subjects were instructed to keep fixated throughout.

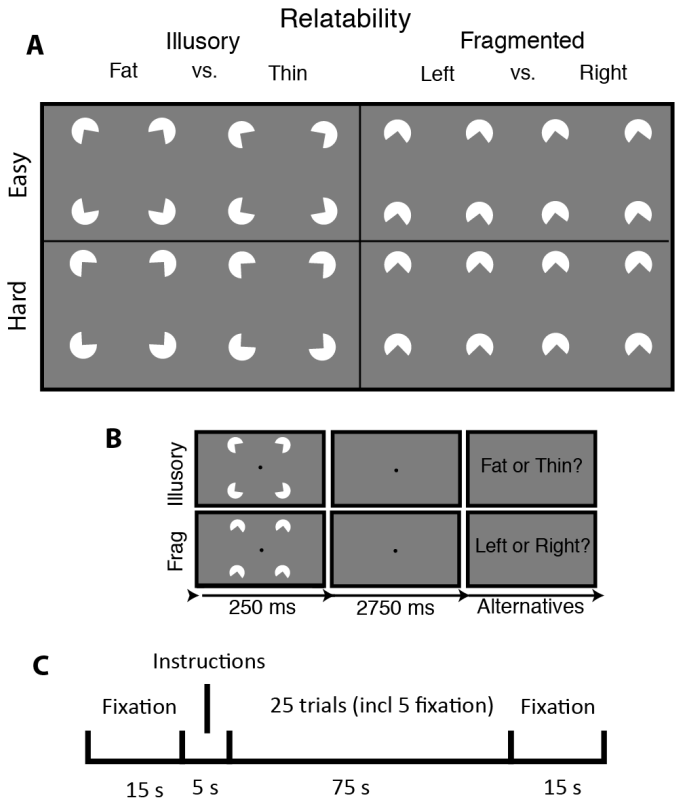

Fig. 1. *Stimuli, trial sequence, and block arrangement for the visual shape completion experiment*. (A) Sectored circles (pac-men) were oriented to generate visually completed shapes (illusory condition) or fragmented configurations that lacked interpolated boundaries (fragmented condition). There were two difficulty conditions corresponding to the amount by which the pac-men were individually rotated to create the response alternatives. (B) After briefly seeing the target, subjects responded. (C) Each half of a run consisted of a fixation screen, a 5 second instructional screen, 25 trials of a single task condition (including 5 fixation trials), and then another fixation screen.

Within each of the four runs, there was one block of each task condition. In the illusory block, subjects indicated whether four pac-men formed a fat or thin shape; in the fragmented block, subjects indicated whether four downward-facing pac-men were each rotated left or right (see Fig. 1). Block ordering (illusory/fragmented or vice versa) alternated from one run to the next. Each block had two difficulty levels, corresponding to the magnitude of pac-man rotation (+/- 10 degrees “easy”, or +/- 3 degrees of rotation, “hard”). Within each block there were 20 task trials and 5 fixation trials. Half of the task trials were easy, and half were hard; half of these two trial types were illusory, and half were fragmented. The ordering of these trial types (including fixation) was counterbalanced. Each trial consisted of a 250 ms pac-man stimulus

(task trial) or 250 ms fixation dot (fixation trial), followed by a 2750 ms fixation dot. Subjects needed to issue a response before the end of a task trial; otherwise, a randomly selected response was assigned, and the following trial ensued. Feedback was provided at the end of each run in the form of accuracy averaged cumulatively across all test trials.

Subjects received brief practice outside of and within the scanner before the actual experiment. To ensure that subjects thoroughly understood the task, pictures of the fat/thin stimuli were shown side-by-side and in alternation so that the differences could be clearly envisaged. Subjects issued responses with a two-button response device that was held on their abdomens with their dominant hand; subjects practiced with this same type of device outside of the scanner facility. Feedback after each trial was provided during the practice only (indicating correct, incorrect, or slow response).

fMRI acquisition. Data were collected at the Rutgers University Brain Imaging Center (RUBIC) on a Siemens Tim Trio scanner. Whole-brain multiband echo-planar imaging (EPI) acquisitions were collected with a 32-channel head coil with TR = 785 ms, TE = 34.8 ms, flip angle = 55°, bandwidth 1894/Hz/Px, in-plane FoV read = 211 mm, 60 slices, 2.4 mm isotropic voxels, with GRAPPA (PAT=2) and multiband acceleration factor 6. Whole-brain high-resolution T1-weighted and T2-weighted anatomical scans were also collected with 0.8 mm isotropic voxels. Spin echo field maps were collected in both the anterior to posterior and posterior to anterior directions in accordance with the Human Connectome Project preprocessing pipeline (Glasser et al., 2013). “Dummy” scans were acquired at the beginning of each run to allow the brain to reach steady-state magnetization. Excluding dummy volumes, each experimental functional scan spanned 3 min and 41 s (281 TRs) and were collected consecutively with short breaks in between (subjects did not leave the scanner). An additional 10 minute resting-state scan (765 TRs) occurred in a separate session, with the same pulse sequence.

fMRI preprocessing. Imaging data were preprocessed using the publicly available Human Connectome Project minimal preprocessing pipeline which included anatomical reconstruction and segmentation, EPI reconstruction, segmentation, spatial normalization to standard template, intensity normalization, and motion correction (Glasser et al., 2013). All subsequent preprocessing steps and analyses were conducted on CIFTI 64k grayordinate standard space. This was done for the parcellated time series using the Glasser et al. (2016) atlas (i.e., one time series for each of the 360 cortical parcels). An advantage of the Glasser

parcellation is that it provides a principled and powerful way to determine what other regions may be critically involved in visual shape completion (versus a whole-brain vertex-wise analysis). The surface-based cortical parcellation combined multiple neuroimaging modalities (i.e., myelin mapping, cortical thickness, task fMRI, and RSFC) to improve confidence in cortical area assignment. An average BOLD time course for each parcel was calculated by averaging across all vertices within that region. To conduct a specific follow-up MVPA analysis within V1 and V2 parcels (see Results), we also performed an otherwise identical preprocessing pipeline on the vertex-wise data. In all cases, we performed nuisance regression on the minimally preprocessed task data using 24 motion parameters (6 motion parameter estimates, their derivatives, and the squares of each) and the 4 ventricle and 4 white matter parameters (parameter estimates, the derivates, and the squares of each) (Ciric et al., 2017). For the task scans, global signal regression, motion scrubbing, spatial smoothing, and temporal filtering were not used. Each run was individually demeaned and detrended (2 additional regressors per run).

The resting-state scans were preprocessed in the same way as the parcellated data (including the absence of global signal regression) except that we removed the first five frames and applied motion scrubbing (Power et al., 2012). Whenever the framewise displacement for a particular frame exceeded 0.3 mm, we removed that frame, one prior frame, and two subsequent frames (Schultz et al., 2018). Framewise displacement was calculated as the Euclidean distance of the head position in one frame as compared to the one preceding.

Functional and anatomical scans were visually inspected for quality. In addition, an MRI quality control package (“MRIQC”) and an accompanying random forest classifier were used to confirm that all T1 anatomical scans were artifact free (Esteban et al., 2017). (Two other participants, not included in our analyzed sample, had been flagged by MRIQC as having low quality T1 scans.) The mean framewise displacement across scans before motion correction or scrubbing was remarkably similar in the visual completion and rest scans: 0.142 mm for visual completion (averaged across scans) and 0.143 mm for rest. The average number of frames remaining after scrubbing for the rest scan was 696 [range: 548-760].

For the task scans, there were 6 task regressors, one for each instructional screen (illusory/fragmented) and one for each of the four trial types (illusory/fragmented, easy/hard). A standard fMRI general linear model (GLM) was fit to task-evoked activity convolved with the SPM canonical hemodynamic response function (using the function spm_hrf.m). Betas for the

illusory and fragmented condition were derived from all trials of the relevant condition across all four runs. For the classifier analyses, described below, task activation betas were derived separately for each run, but all other steps were the same as described.

Analyses

Analyses were performed with RStudio (Version 1.2.1335) and MATLAB R2018b; cortical visualizations were created with Workbench (version 1.2.3). There were eight parcels of a priori interest in each hemisphere. These ROIs have been given different names in different research studies (shown in parentheses) and are as follows: V1 (17, hOC1, OC, BA17), V2 (18, hOC2, OB, BA18) , V4 (V4d, V4v, hV4, hOC4v, hOC4lp), V4t (LO2), LO1 (LO2, hOC4la); LO2 (LO1, hOC4la), LO3 (hOC4la), and V3CD (V3A,V3B, hOC4la) (Glasser et al., 2016 p.81 see of Supplementary Neuroanatomical Results). Note that V3CD was included because it corresponds to the anterior third of the middle and inferior lateral occipital gyri (area hOc4la as labeled by Malikovic et al., 2016). Statistical correction, when applied, was via the False Discovery Rate (FDR) method (Benjamini and Hochberg, 1995). For the univariate task activation analysis, regions that were and were not of a priori interest were separately FDR-corrected. (Statistical correction is indicated explicitly in the text below, e.g., via p_{corr} values).

For the group-level task activation analyses, betas were derived for each parcel and subject, averaged across difficulty condition, subtracted (illusory-fragmented), and then compared to zero (across subjects) with a one-sample t-test. As a control analysis, we did the same as just described, except that we averaged across *task* condition and contrasted the easy/hard conditions. Individual subject parcel-wise task activation analyses were also performed for the illusory/fragmented contrast (e.g., Table 1), using the subject's estimated covariance matrix, task betas, and MATLAB's linear hypothesis test function (linhyptest).

The location and role of each parcel was considered in the context of their functional network affiliations. We used a recent network partition that comprised 12 functional networks; these were constructed from the above-mentioned parcels and were defined via a General Louvain community detection algorithm using resting-state data from healthy adults (Ji et al., 2019 see Figure 4A).

Multivariate pattern analysis was performed on the activation betas at two levels of spatial granularity. First, we examined whether 12 different functional networks could individually

classify task condition (illusory vs fragmented) or difficulty condition (easy vs hard) using their within-network mean parcel activations as features. Next, we examined, for each parcel, whether vertex-wise activations could classify task condition. MVPA classification accuracy in both cases was assessed via leave-two-runs-out cross validation. For example, when classifying task condition for each participant, we examined whether the betas for each of the two left-out runs better correlated to the averaged illusory or fragmented betas of the remaining runs. Note that each run contained each of the two conditions, ensuring balanced condition types across test and training. Pearson correlation served as the minimum distance classifier (i.e., 1-r) (Mur et al., 2009; Spronk et al., 2018). Results were averaged for each subject across the 6 possible ways to divide the four runs between test and validation. Statistical significance was determined via permutation testing, which generated a null distribution of classification accuracies through the same procedure with 10,000 samples. That is, for each sample, the "illusory" and "fragmented" labels were shuffled for each subject and run, and the classification results were averaged across subjects and across the 6 possible divisions of testing and validation data sets.

Resting-state functional connectivity matrices. We determined the resting-state functional connections for each parcel. Specifically, for each target parcel time series, we decomposed the time series of the remaining (N=359) parcels into 100 components, regressed the target onto the PCA scores, and back-transformed the PCA betas into a parcel-wise vector. The average amount of variance explained by the components across subjects was 84% [range: 81-88%]. The RSFC computation is equivalent to running a multiple regression for each parcel, with all other parcels serving as regressors. An advantage of using multiple regression is that it removes indirect connections (Cole et al., 2016). For example, if there exists a true connection from A to B and B to C, a Pearson correlation, but not regression, would incorrectly show connections between A and C. PC regression was preferred over ordinary least squares to prevent over-fitting (using all components would inevitably capture noise in the data).

Activity flow mapping. Figure 6 illustrates how we used resting-state data to predict task activation ("Activity Flow mapping" or simply "ActFlow"), where the "activations" in this case correspond to the illusory-fragmented difference. For each subject, task activations in a held-out parcel ('j' in Figure X) was predicted as the weighted average of the activations of all other

parcels, with the weights being given by the resting-state connections. That is, for each subject, each held out region's predicted value was given as the dot product of the task activations in the remaining regions ('i' in Figure 6A) and the subject's restFC between j and i (using the FC weight from the appropriately oriented regression, i.e. j as the target and i as the predictor). The accuracy of the activity flow predictions was then assessed by computing the overlap (Pearson correlation) between the predicted and actual task activation difference vector. Overlap can be expressed by comparing actual and predicted activations for each subject, and then averaging the resulting Fisher-transformed r values (r_z) across subjects (subject-level overlap). Statistical significance can be determined by comparing the vector of r_z values to zero via a one-sample t-test. Overlap can also be expressed by averaging the predicted values across subjects and then comparing that to the averaged actual values, which will yield a single Pearson r value (group-level overlap).

Results

Below, upon reporting the behavioral results, we report parcel-wise task activation analyses to determine the regions most associated with shape completion. We then quantify each network's contribution to shape completion by applying MVPA to within-network parcel-wise activation patterns for the two task conditions. Null task activation results in V1 and V2 prompted us to additionally apply MVPA to within-parcel vertices to probe for fine-grained patterns of shape completion. To determine how parcels potentially interacted, we computed the resting-state functional connectomes (RSFC matrices) and then demonstrated the likely utility of these connections for shape completion via ActFlow. We conclude by suggesting the existence of a shape completion network coalition, which is seated in the secondary visual network, is orchestrated by the dorsal attention network, incorporates pieces of three other networks, and interacts with early visual areas at a vertex-wise spatial resolution.

Behavioral task performance

Employing a 2 (task condition) by 2 (difficulty) within-subjects ANOVA (type III sum of squares), we found that performance was better in the fragmented than illusory condition (89.2% versus 82.8%, $F(1,19)=14.8$, $p=.001$). The large rotation ("easy") condition yielded better performance than the small rotation condition ($F(1,19)=133$, $p<10^{-9}$). The accuracy

difference between illusory and fragmented conditions did not depend on difficulty level, although there was a trend toward greater differences on the smaller rotation condition (two-way interaction: (F(1,19)=3.6, p=.07). No-response trials were infrequent, occurring on only 5.5% of the trials on average. The frequency of no-response trials did not vary with difficulty level or task condition nor was there an interaction between difficulty and task condition (ps>.25).

Task activation effects of shape completion across five different networks

A general linear model task activation analysis determined the parcels that were differentially active in the illusory versus fragmented condition. Overall, there were 34 parcels reached significance in five different networks (Table 1). Of these, 26 (76 percent) were more activated for illusory relative to fragmented trials (Figure 2). A priori ROIs, when significant, were all more active relative to the control condition; these include bilateral V3CD, V4, L01, and left L02. These effects were robust and would also be significant if we simply performed a cortex-wide FDR correction. Notable null results were V2 and V1 which will be discussed further below. Additional positively and significantly activated regions resided in the posterior parietal, dorsolateral prefrontal, and orbitofrontal regions; they belonged primarily to the secondary visual, dorsal attention, and frontoparietal networks. All 8 of the regions that displayed less relative activation in the illusory-fragmented contrast belonged to the default mode network. Note that this finding reflects this network's established on-task deactivation profile (Anticevic et al., 2012), i.e. greater deactivation for the illusory relative to the fragmented condition, consistent with greater engagement in the illusory condition.

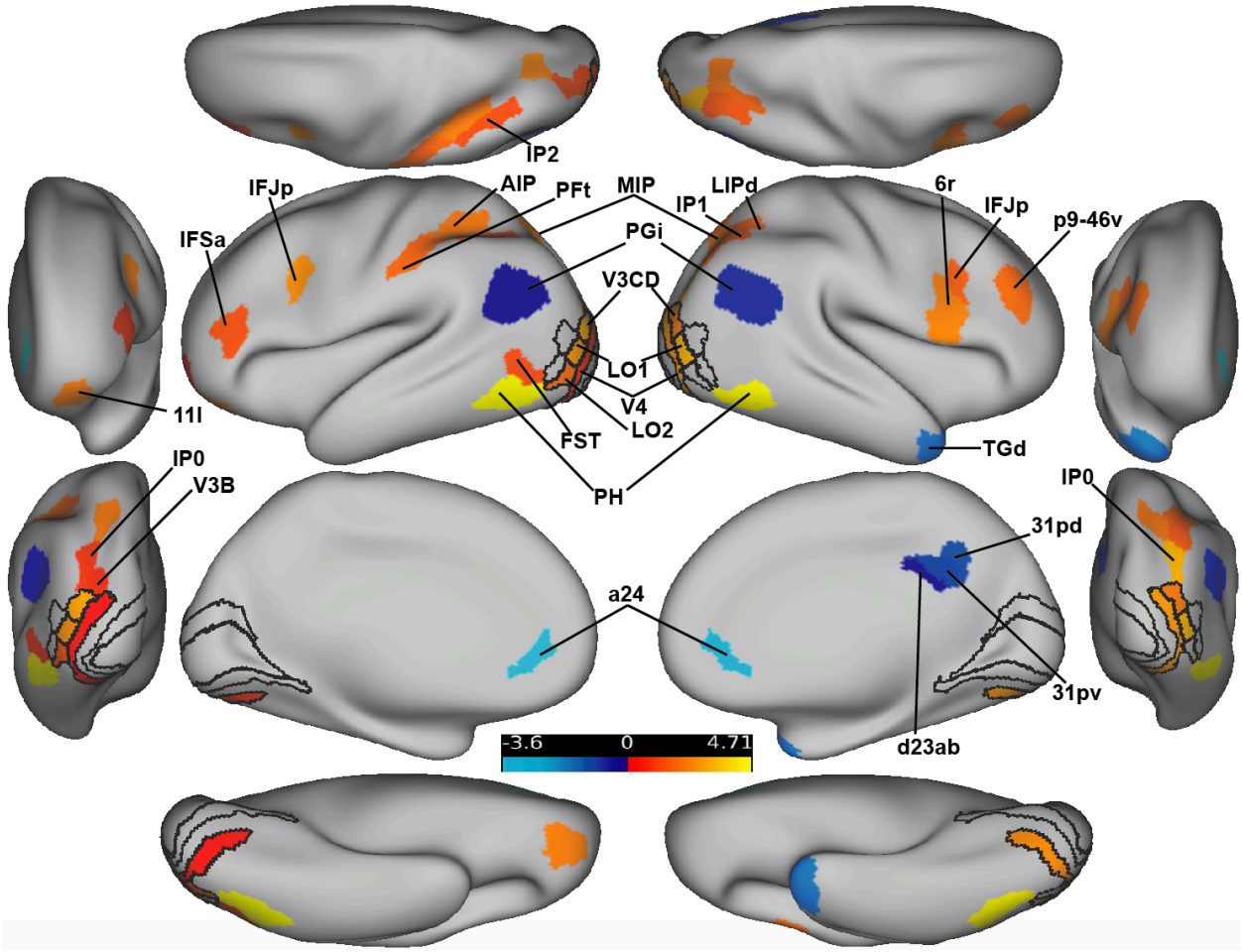

Fig. 2. FDR-corrected activation difference amplitudes (Z-normalized) for all parcels for the illusory – fragmented contrast. ROIs are shown with black outlines. The anterior and posterior views are shown laterally; the dorsal and ventral views are shown at the top and bottom. Hot colors indicate regions that were more active for the illusory versus fragmented task; cool colors indicate the reverse.

Because task difficulty was greater in the illusory task, perhaps task difficulty, rather than shape completion, drove the effects just described. We addressed this concern in two ways. First, we performed a contrast comparing activation in the easy versus hard trials, averaged across task conditions. To make the results comparable to before, FDR correction was applied separately to regions that were and were not ROIs. We found 17 parcels that were differentially active, but only four overlapped with the illusory-fragmented contrast (see Fig. 3). Three of these parcels were less active in both the hard-easy and illusory-fragmented

comparisons: right d23ab, right TGd, and right PGi; one was more active in both (right IFJp). None of the 16 ROIs of visual shape completion were related to task difficulty. Thus, on this analysis, while the above-mentioned four parcels were confounded with task difficulty, the remaining 30 significant parcels in the illusory/fragmented comparison were not confounded.

To further assess the extent to which task difficulty might account for the aforementioned shape completion effects, we ran an additional analysis that was restricted to the 10 participants who did the best in the illusory relative to the fragmented condition, so that there was no longer an accuracy difference ($t(9) = -0.443$, $p=0.669$, Mean difference in proportion correct=-0.011). In this sample, there was also no reaction time difference between task conditions ($t(9)=1.63$, mean RT difference=-.06 seconds, $p=.14$)). As shown in Table 1, the ROIs that were significant in the earlier analysis remained significant in this restricted sample; these include L01 and V3CD in each hemisphere, left LO2 and orbitofrontal region (11l), and right V4 (all $p<.05$, uncorrected). Of the four regions that were significant on both the hard/easy and illusory/fragmented contrast (right d23ab, right PGi, right TGd, right IFJp), only right TGd remained significant and thus is more plausibly independent of task difficulty. Other regions that continued to be significant are shown in Table 1.

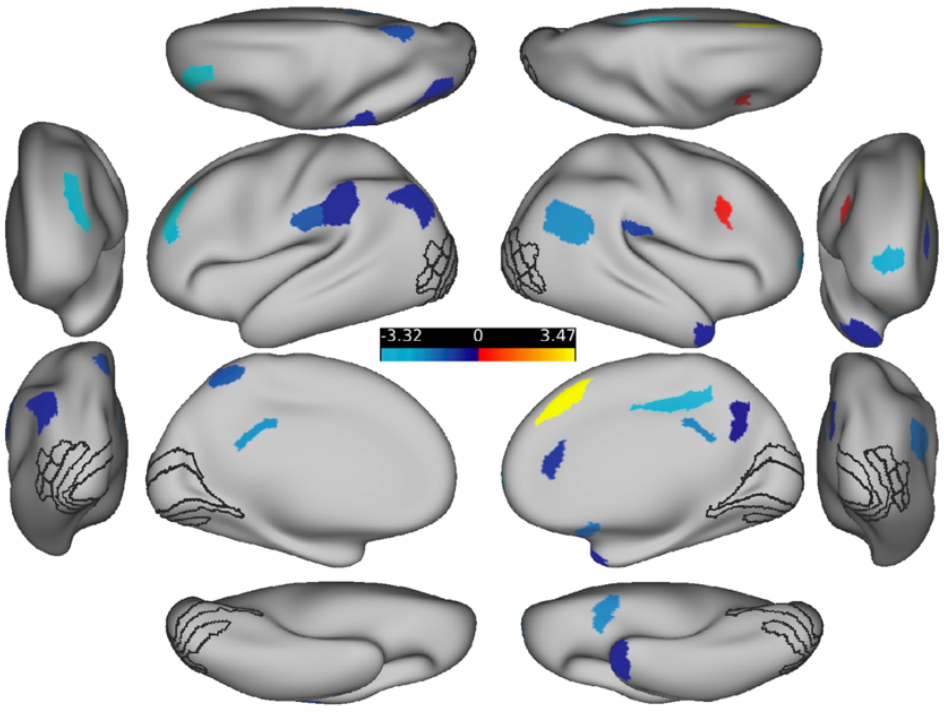

Fig 3. *Task activation differences for hard - easy trials.* Opposite to the illusory-fragmented contrast, we found that harder trials generally elicited less activation throughout the brain relative to easier trials and the location of these significant activations overlapped little with the activations shown in Figure 2. The illusory/fragmented ROIs (black outlines) are shown for comparison purposes only and did not contain significant parcels.

To examine the robustness of the task activation effects, we additionally report the percentage of subjects showing significant effects (illusory-fragmented) in the group direction on an individual subject analysis (with a linear hypothesis test, see Methods). This was done for regions that were significant on the task activation analysis as well as for other regions that were of a priori interest. As can be seen from Table 1, about 80% of parcels (ranging from 70-100%, depending on the parcel) showed activation differences in the group direction and about half (35 - 80%) showed effects that were statistically significant. Intriguingly, the inferior lateral temporal region PH–which was not of a priori interest—was *most* associated with shape completion, with 80% showing a significant effect in the left hemisphere and 70% in the right hemisphere, and with at least 95% showing differences in the group direction in the left and the right hemispheres. As will be shown further below (Figure 5), of all the significant visual regions, PH was the most densely interconnected.

Parcel Name	% With Difference In Group Direction	% With Sig. Difference	ROI?	Network	Sig. with FDR correction?	Sig. with accuracy matching ?	Sig. with Act-Flow?	Mean Beta Difference [95% CI]
R_PH	100	70	0	Visual2	1	1	1	111.5 [75.6,147.5]
L_PH	95	80	0	Visual2	1	1	1	93.2 [63.7,122.7]
L_MIP	95	60	0	Dorsal-attention	1	1	1	80.8 [41.9,119.7]
R_V4	95	55	1	Visual2	1	1	1	47.4 [25.7, 69.1]
L_IFJp	90	50	0	Frontoparietal	1	1	1	87.5 [45.8,129.2]
R_p9-46v	90	50	0	Frontoparietal	1	1	1	60.5 [27.4, 93.5]
L_LO1	90	40	1	Visual2	1	1	1	66.7 [36.4, 97.1]
R_a24	90	35	0	Default	1	1	1	-44.5 [-66.2,-22.9]
L_V3CD	85	75	1	Visual2	1	1	1	76.1 [43.8,108.3]
L_PFt	85	60	0	Dorsal-attention	1	1	1	60.5 [26.5, 94.5]
R_IP0	85	60	0	Dorsal-attention	1	1	1	76.1 [44.7,107.6]
R_V3CD	85	60	1	Visual2	1	1	1	67.8 [32.9,102.8]
L_V4	85	55	1	Visual2	1	0	1	41.0 [13.6, 68.3]
L_a24	85	55	0	Default	1	1	1	-49.5 [-73.1,-25.8]

R_LIPd	85	55	0	Dorsal-attention	1	1	1	78.8 [34.6,123.1]
R_TGd	85	50	0	Default	1	1	1	-36.4 [-56.9, -16.0]
L_IP0	85	45	0	Dorsal-attention	1	0	1	64.1 [25.3,102.8]
R_LO1	85	45	1	Visual2	1	1	1	58.5 [34.4, 82.5]
R_PGi	85	45	0	Default	1	0	1	-40.0 [-64.5,-15.4]
R_IFJp	85	40	0	Frontoparietal	1	0	1	85.2 [36.5,133.8]
L_IFSa	85	35	0	Frontoparietal	1	1	0	48.5 [19.3, 77.7]
R_31pd	85	35	0	Default	1	0	1	-60.1 [-95.8,-24.4]
L_PGi	85	30	0	Default	1	0	1	-36.8 [-60.1,-13.5]
L_AIP	80	60	0	Dorsal-attention	1	1	1	76.7 [37.0,116.4]
L_11l	80	55	0	Frontoparietal	1	1	1	60.6 [31.8, 89.4]
R_MIP	80	55	0	Dorsal-attention	1	1	1	79.1 [37.7,120.5]
R_6r	80	55	0	Cingulo-Opercular	1	1	1	53.0 [26.6, 79.5]
L_V3B	80	50	0	Visual2	1	1	0	52.0 [19.5, 84.5]
L_LO2	80	45	1	Visual2	1	1	1	50.4 [23.1, 77.7]
R_LO2	80	45	1	Visual2	0	0	1	47.3 [5.7, 88.8]
L_FST	80	35	0	Visual2	1	0	1	46.7 [17.8, 75.5]
L_IP2	75	60	0	Frontoparietal	1	1	1	70.9 [27.0,114.7]
R_d23ab	75	30	0	Default	1	0	1	-53.9 [-88.1,-19.7]
R_IP1	70	55	0	Frontoparietal	1	0	0	52.1 [21.8, 82.4]
L_LO3	70	35	1	Visual2	0	0	1	26.6 [-12.3, 65.6]
R_31pv	70	30	0	Default	1	0	1	-54.8 [-87.7,-21.9]
R_LO3	70	30	1	Visual2	0	0	0	22.9 [-13.5, 59.4]
R_V4t	70	25	1	Visual2	0	0	0	16.8 [-21.2, 54.9]
R_V2	60	25	1	Visual2	0	0	0	3.2 [-30.0, 36.4]
L_V2	60	20	1	Visual2	0	0	0	7.0 [-23.4, 37.3]
L_V1	55	30	1	Visual1	0	0	0	9.1 [-25.4, 43.7]
R_V1	55	25	1	Visual1	0	0	0	7.0 [-28.3, 42.2]
L_V4t	50	15	1	Visual2	0	0	0	-0.2 [-34.9, 34.5]

Table 1. *Results for parcels that that were either of a priori interest or that were significant on the illusory-fragmented task activation analysis* (see Figure 2). The rows were sorted in descending order, first, by the percentage of subjects showing the effect in the group direction (column 2) and, then, by the percentage of subjects showing significant effects on the individual subject analysis (column 3). The prefix of each parcel name ("L_ "or "R_") indicated its hemisphere. The fourth and fifth columns indicate a parcel's ROI status (yes/no) and functional network. The next three columns indicate whether a parcel was significant after FDR correction, whether it remained significant when task conditions were matched on accuracy/RT, and whether it was significant using the predicted ActFlow data. In the final column, we show the average task activation difference, with more positive values indicating more illusory relative to fragmented activation.

A dominant role for the secondary visual network in shape completion

As shown in Table 1, 32% of the significant parcels were in the secondary visual network, which was followed by the default mode (24%), dorsal attention (21%), frontoparietal (21%), and cingulo-opercular networks (3%). To better quantify the network contributions and compare them to one another, we trained MVPA classifiers separately for the 12 functional networks (Ji et al., 2019), using parcel-wise activations as features (see Methods). After FDR correction (across tests for the 12 networks), the secondary visual could reliably distinguish the illusory and fragmented conditions (p_{corr}=.004, accuracy=63%), but no other network could do so (all p_{corr}>.24). Paired t-tests showed that after FDR correction the secondary visual network was marginally more predictive than 8 of the remaining 11 networks (all p_{corr}<.10). Note that there was no correlation between network classification accuracy and parcel count (r=.001, p=.997), suggesting that smaller networks were not unduly handicapped.

To assess whether the classification success of the secondary visual network was specific to shape completion and also whether the other networks could be predictive under different circumstances, we additionally ran network-level classifications that distinguished between easy and hard trials. Six networks came out as significant: somatomotor (p_{corr}=.03, accuracy=56%), cingulo-opercular (p_{corr}=.005, accuracy=60%), dorsal attention (p_{corr}=.007, accuracy=57%), language (p_{corr}=.03, accuracy=56%), frontoparietal (p_{corr}=.004, accuracy=60%), and posterior multimodal (p_{corr}=.03, accuracy=56%). Neither of the visual networks were significant. Thus our data set and analytic approach could reveal significant effects for a number of networks, but only the secondary visual was relevant when examining visual shape completion. Taken together, these results suggest that—purely from the perspective of parcel-wise task activation differences—the secondary visual network played a robust, specific, and outsized role in shape completion.

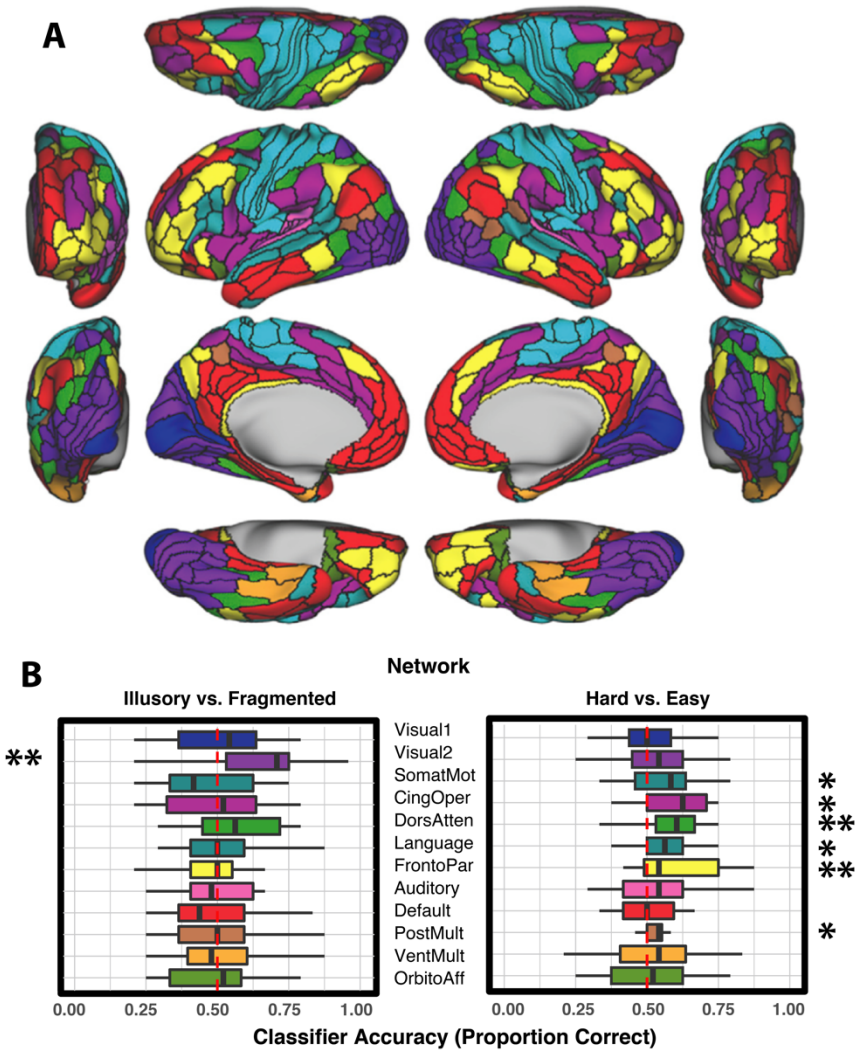

Fig. 4. (A) Functional network partition for the network-level multivariate pattern analysis. We considered whether parcel-wise activation patterns in twelve cortical networks could individually classify task betas as deriving from the illusory or fragmented condition; these included the primary visual, secondary visual, somatomotor, cingulo-opercular, dorsal attention, language, frontoparietal, auditory, default, posterior multimodal, ventral multimodal, and orbito-affective networks. (B) Classification accuracy for the illusory/fragmented and hard/easy comparisons. Networks are color coded to match the parcels in panel A. The red dotted line shows chance performance, the box segments denote median scores, the box hinges correspond to the 25th and 75th percentiles, and the box whiskers extend to the largest or smallest value (but no further than 1.5x the interquartile range). Only the secondary visual network could significantly predict illusory/fragmented activations. In comparison, multiple networks were involved in classifying easier/harder trials, after FDR correction (*p_{corr}<.05, ** p_{corr}<.01).

Fine-grained multivariate traces of shape completion in early visual cortex

Our task activation analyses did not reveal shape completion effects in V1 or V2, which were ROIs. Because a region could conceivably encode a completed shape in the multivariate pattern of its constituent vertices rather than the univariate mean across them (Haynes, 2015), we performed MVPA on vertices within these parcels. For completeness, we considered effects within all 360 parcels. The following were significant: L_V4 (p=.02, accuracy=58%), L_LO2 (p=.03, accuracy =56%), L_V3CD (p=.02, accuracy=58%), R_V1 (p=.03, accuracy=56%), R_V4 (p=.01, accuracy=57%), and R_LO2 (p=.03, accuracy=56%). These effects were not corrected for multiple comparisons but are credible given the strong prior evidence for their involvement (see Introduction). Outside of the ROIs, the only region that was significant after FDR correction was R_PGp (p=.03, accuracy=64%). Given the hemispherically similar task activations and the bilateral stimulus displays, we performed the same analysis as above, except that vertices were aggregated (without averaging) across hemisphere to increase sensitivity. The effects were similar to before with effects for: V1 (p=.027, accuracy=57%), V4 (p=.014, accuracy=58%), LO2 (p=.01, accuracy=58%), and LO3 (p=.03, accuracy=56%). For regions that were not of a priori interest, the following reached significance after FDR correction: PGp (p_{corr}<.0001, accuracy=62.9%) in the secondary visual network and IP1 in the frontoparietal network (p_{corr}=.04, accuracy=61%). In sum, V1 but not V2 exhibited modest vertex-wise shape completion effects; additional ROIs (V4, LO2) and a new region, PGp, were also consistently significant on this analysis.

Significantly activated task parcels are functionally inter-connected during rest

We sought to determine not only what regions were modulated but also how those regions connected to one another. Towards this end, a resting-state functional connectivity estimation was performed with the more standard Pearson correlation approach (Figure 5A) and then with multiple regression (Figure 5B; see Methods). The predicted parcel-wise betas of the latter method were compared to zero for each parcel (one sample t-test), and the FDR-corrected (thresholded) map is shown in Figure 5C. After examining whole-cortex functional connections, we homed in on the regions that were significant on the task activation analysis and that remained significant when the illusory/fragmented conditions were matched on

accuracy/RT. Contralateral homologues were included since the task activations were hemispherically symmetric. This means that the total number of regions included in the RSFC matrix was 38.

Six observations will inform the discussion below. First, as an initial sanity check, informal observation of Figure 5C shows that parcels had: higher within- than between-hemisphere RSFC, more cross-hemisphere connections for sensory (visual) than for non-sensory networks, and high RSFC with their contralateral homologues, which is consistent with past work (Stark et al., 2008; Power et al., 2011). Second, the 38 task activation regions on this analysis were remarkably inter-connected during rest. After applying FDR corrections to each matrix separately, the restricted RSFC matrix (38 x 38) contained three times as many significant resting-state connections as the full (360 x 360) matrix, (39.6 % versus 13.5%). To put this in perspective, two of the twelve resting-state networks—default mode and orbitoaffective—had a lower proportion of significant *within*-network connections (35% and 25%, respectively). This suggests that the significant task regions, despite being composed of five different networks, composed a densely inter-connected network coalition or supra-network. Note that these five networks were not unusually connected to one another: If all regions from all 5 networks were included in the above calculations (to form a 260 x 260 RSFC matrix), the total number of significant resting state connections would still only be 17%. Thus, it is the specific regions within these five networks that appear to be more interconnected during rest.

A third observation is that although the significant secondary visual network parcels were generally modular (having 4.6 times as many intrinsic relative to extrinsic network connections), area PH was a glaring exception, connecting to the cingulo-opercular, frontoparietal, and dorsal attention networks. Fourth, as will be fleshed out further below and as can be gleaned from inspection of Figure 5D, when the secondary visual network did connect to other regions, it was most typically to dorsal attention regions. Fifth, as is evident from that same Figure, the significant dorsal attention network regions had the most significant out-of-network connections (117 connections), suggesting a possible role for orchestrating activity in the remaining networks. Finally, there appear to be a number of routes between frontal cortex and the mid-level vision ROIs. Dorsal lateral prefrontal cortex (p9-46v) connects with MIP, IPO, and IP2 (in posterior parietal cortex), which in turn connect with all of the

significant ROI regions. Intriguingly, area 11l (OFC) connected directly with area LO2. Hence there exist clear routes for conceptual or value-laden information to loop back into areas most typically associated with visual shape completion.

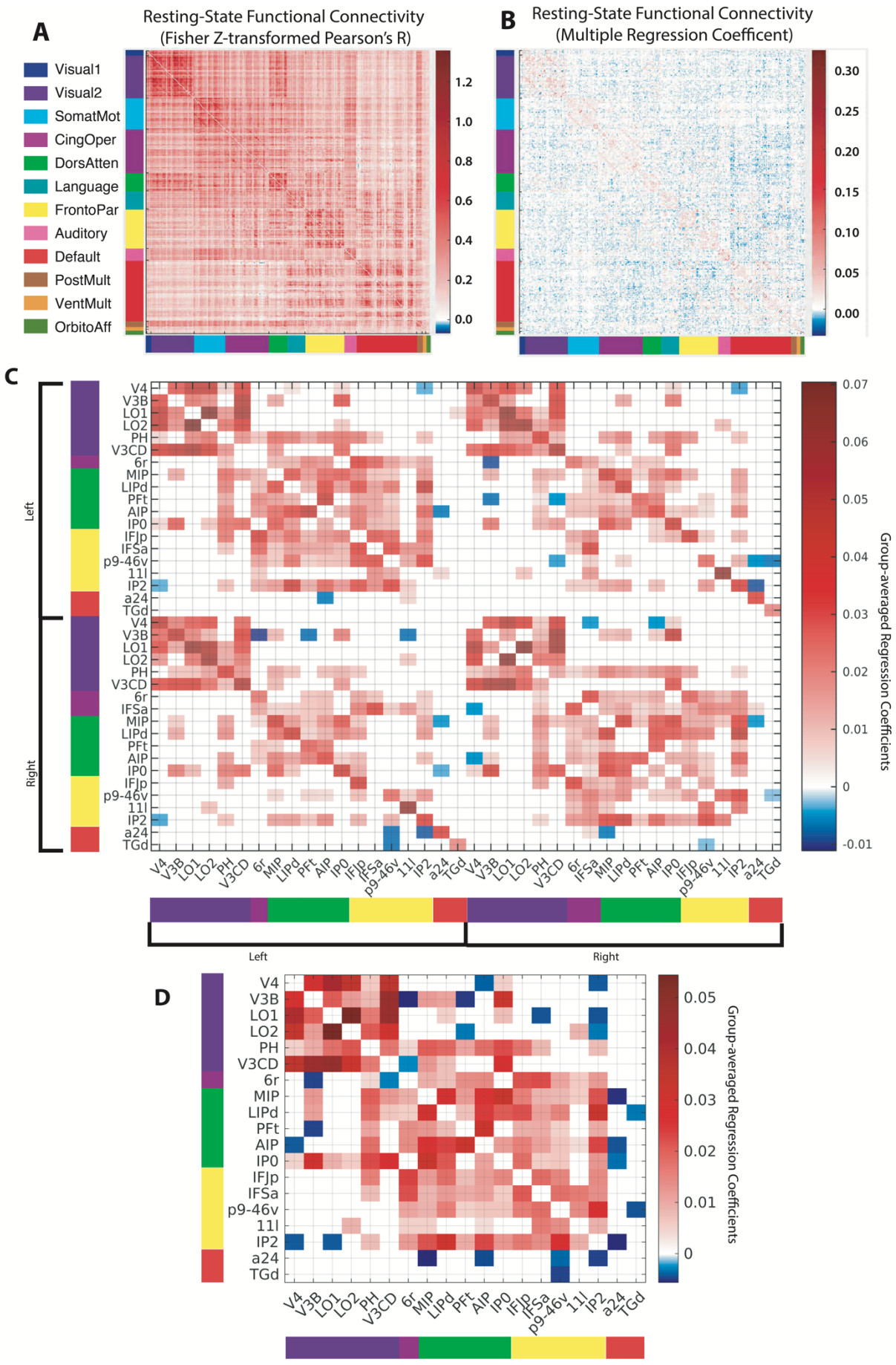

Fig. 5. *Resting-state functional connectivity (RSFC) matrices*. (A) Pearson correlation between the resting-state time series of parcel pairs for all 360 parcels. Parcels are sorted into previously established (color-coded) functional connectivity networks (Ji et al., 2019) (see also Figure 4A). The block-like structure along the diagonal exemplifies the stronger connectivity within relative to between each network. (B) An RSFC matrix computed via multiple regression (see Methods). The blue/red colors indicate the degree to which a given parcel time series was predicted by all remaining parcels. Note that this matrix is much sparser than the correlational matrix since it eliminates many of the indirect connections between parcels (Cole et al., 2016). (C) Thresholded (FDR-corrected) resting-state connections between regions that remained significant on the task activation analyses (see text). The regions are ordered first by hemisphere and then by network. Compared to the full matrix in panel B, this pared down matrix had about 1 percent the number of possible connections (matrix elements) and triple the proportion of (FDR-corrected) significant connections. (D) Averaging the connection weights across hemisphere increased the proportion even further (from 40% to 53%), highlighting the broadly symmetric connectivity patterns. Note that one parcel, IFSa, was split between the frontoparietal (left hemisphere) and cingulo-opercular networks (right), and was assigned to the frontoparietal network in this plot since only the frontoparietal parcel was significant in the task activation analysis.

Resting-state connections are relevant for visual shape completion

So far, we have shown that regions that were differentially activated during visual shape completion were also connected during rest. We have descriptively sketched plausible routes by which frontoparietal regions can communicate with mid-level vision. However, despite some indirect evidence from other work (see Introduction), it remains unclear whether these connections in these same subjects played a mechanistic role in shape completion. To address the question, we leveraged a recently-developed predictive modeling approach—activity flow mapping ("ActFlow")—to assess whether the multiple regression resting-state connections were likely instrumental in carrying the flow of activity between regions during task performance (Cole et al., 2016). In this method, the activation difference (illusory minus fragmented) in a held-out "target" parcel was computed as the linear weighted sum of the activation differences in all other parcels, with the weights being given by the resting-state connections to the target (see Figure 6a). This can be thought of as a rough simulation of the movement of task-evoked activity between brain regions that likely contributed to each brain region's task-evoked activity level. This allowed us to assess whether the observed resting-

state connections mechanistically supported the perceptual processes associated with the predicted task-evoked activations – in this case shape completion. Prediction accuracy was gauged as the correlation between the actual and predicted activation differences. As can be seen in Figure 6B, the predictions were highly significant at the whole-cortex level ($r=.62$, $p<10^{-9}$). If we were to first average the predicted and actual activation differences across subjects and then correlate those averaged values, the resulting group-level accuracy estimate would increase ($r=.88$), probably by increasing the signal-to-noise ratio (Cole et al., 2016). We next applied a task activation analysis to the ActFlow predicted data (via one-sample t-tests, as before); these results were then compared to the original task activation results (shown in Figure 2). The percentage of parcels that remained significant (sensitivity) with ActFlow was 92%; the percentage of non-significant parcels that remained non-significant (specificity) was 82% (see Figure 6C). These results suggest that the observed resting-state connections describe the routes over which task-evoked activity flows during shape completion (controlling for orientation judgement).

To assess the relevance of resting-state connections between significant task activation regions, we restricted activity flow mapping only to those regions and their contralateral homologues. To minimize the chance of task difficulty effects, we again used only regions that remained significant when conditions were matched on accuracy/RT so that each held-out parcel's activation was predicted by 37 other connections/parcels. Despite cutting 90 percent of the connections for each parcel, the prediction accuracy estimates (r-values) across subjects was still high (illusory-fragmented: $r=.58$, $p=5.8*10^{-8}$) and did not significantly differ ($p=.36$) (as assessed with a paired t-test). Thus, ActFlow predictive accuracy did not depend on whether we had used all 360 regions and the full RSFC matrix or the 38 significant task regions and the 38x38 RSFC matrix. This further underscores the high connectivity of these task regions to one another.

Dorsal attention regions can model activity flow in the secondary visual network and across all other networks

According to the task activation and network-wise MVPA results (Table 1 and Figure 4, respectively), shape completion was most undergirded by the secondary visual network. To examine which other networks might plausibly contribute to the illusory/fragmented activation

differences in this network, we determined which other networks could improve the ActFlow predictions for that network, using the same significant task regions as before. The dorsal attention improved the predictions for the secondary visual network ($\Delta r \approx \Delta r_Z$ =.35, p_{corr}=.01).

Is there a particular network that plays a dominant role in orchestrating the activity of the other regions? We examined this possibility by calculating, for each subject, the ActFlow accuracy for all regions outside of a held-out network and considered how that accuracy improved—that is, how the Fisher-Z correlations increased (Δr_Z)—when the held-out network regions were allowed to contribute (Mill et al., 2020). This was done for each of the five networks, using only the significant task regions (viz., 38 regions were treated as targets for ActFlow in Fig 6A). Consistent with observations from the functional connectivity matrix, the dorsal attention network's contributions significantly improved predictions for the significant regions of all four remaining networks ($\Delta r \approx \Delta r_Z$=.13; t(18)=4.83, p_{corr}=.0007). Interestingly, every other network—including the secondary visual—failed to influence the results on this analysis (all p_{corr}>.17). The improvement from the dorsal attention regions was significant even if we were to use all 360 regions and all possible resting-state connections (rather than restricting to the significantly activated regions; $\Delta r \approx \Delta r_Z$=.03; t(18)=3.60, p_{corr}=.007).

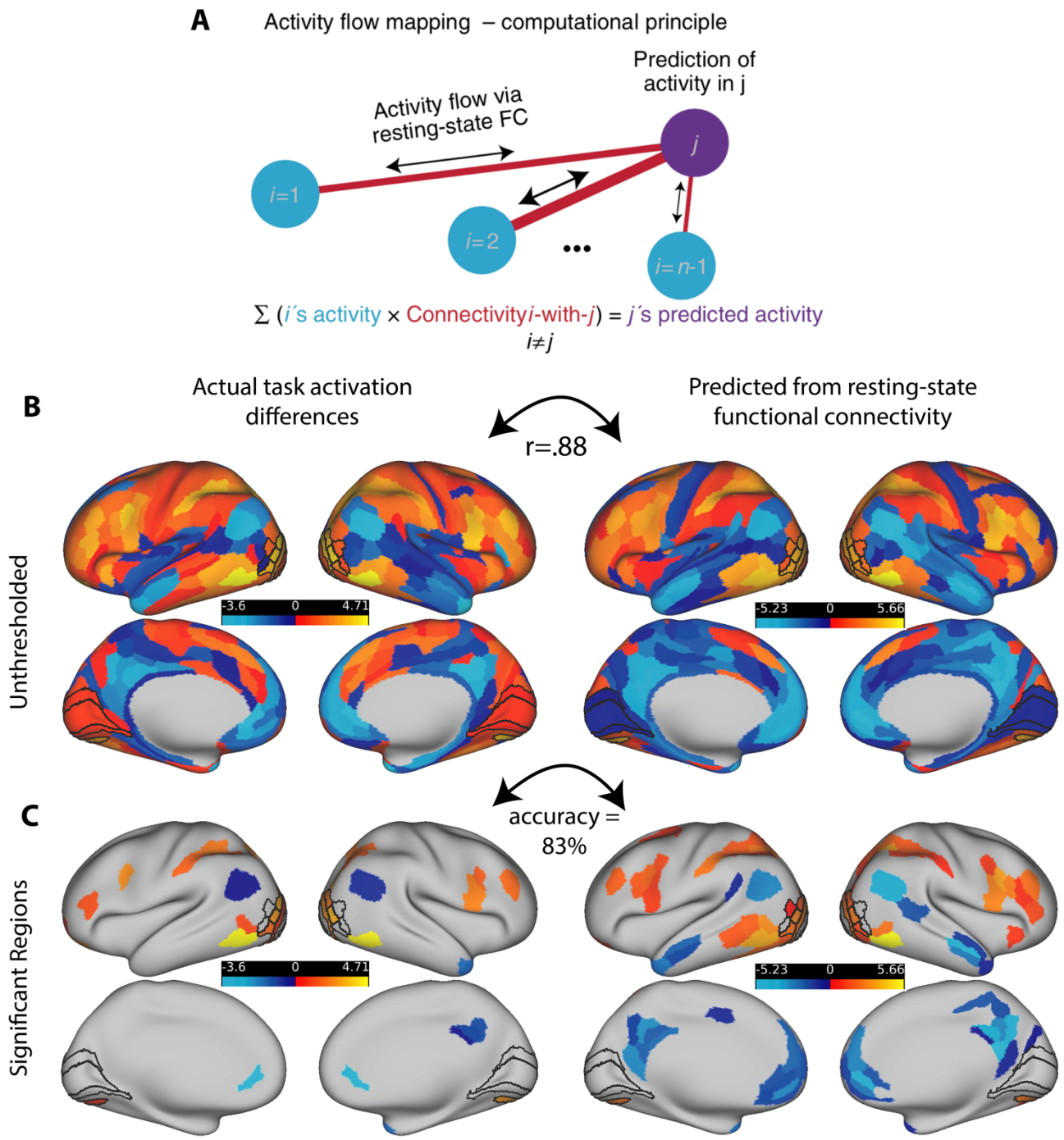

Figure 6. Activity flow mapping for visual shape completion. (A) For each subject, the task activation differences (illusory-fragmented) in a held-out parcel (j) is given by the dot product between the activation differences in the remaining parcels (regions i) and the resting-state connection strengths (betas) between i and j. (B) Unthresholded z-normalized activation differences (illusory – fragmented) as compared to those that were predicted via ActFlow using resting state. (C) When a task activation analysis was applied to the data predicted from ActFlow, statistical significance (or lack thereof) was

correctly determined for 83% of the 360 parcels (see also Figure 2). This suggests that the connection weights derived from resting state are reflective of the actual connections used during shape completion.

Discussion

Visual shape completion recovers object shape, size, position, and number from seemingly inconsequential edge elements dispersed across the field of view. Previous reports suggest that the process relies on lateral occipital and early visual areas, but it is unknown what other regions might be utilized, how they are functionally connected, or what networks they reside within. To shed light on the foregoing, we employed a well-validated "fat/thin" task in which subjects discriminated illusory or fragmented shapes. Compared to earlier neuroimaging studies of shape completion, ours had a well-motivated control condition, a larger and more diverse subject sample, higher spatial and temporal resolution, a surface- rather than volume-based analysis, and a cortical parcellation schema and network partition to mitigate the statistical impact of multiple comparisons. A RSFC analysis coupled with a recent brain activity flow mapping procedure ("ActFlow") enabled inferences as to how task regions were functionally connected. We identified a relatively small number of differentially active task regions that were distributed across five functional networks and that were highly inter-connected during rest. While the secondary visual network played a dominant role in the task activation analyses, dorsal attention regions were also influential in modelling task activity within the secondary visual network and across all remaining networks. Below, we discuss these findings in more detail, provide a sketch of how these regions might interact during shape completion, identify potential limitations, and suggest future directions.

A central role for visual networks in shape completion

Our results confirm past work showing the centrality of visual cortex for shape completion. The secondary visual network contained 32 percent of all significantly activated parcels and parcel-wise patterns across this network, but not other networks, could classify task condition. *A priori* regions of interest—V4, LO1, LO2, LO3, V3CD—were all significant in at least one hemisphere on the task activation analysis; V4 and LO2 were all significant in at least one hemisphere on the vertex-wise MVPA analysis. One surprise was area PH, which

was the most densely inter-connected visual region, the most consistently active parcel across subjects, and the most frequently significant parcel within subject. Signal leakage or imprecise localization of this region could potentially explain significant activations occasionally reported in the immediately adjacent face complex (Larsson et al., 1999b; Halgren et al., 2003).

The primary visual network region, V1, was significant only on a vertex-wise MVPA analysis. A likely reason is that—according to a population receptive field mapping approach (Kok and de Lange, 2014)—the illusory shape surface region (corresponding to a portion of V1/V2 vertices) is more activated in V1 relative to baseline and the inducer (pac-man) regions are *less* activated. Therefore, averaging across these two retinotopic region types will reveal no changes in overall activity. Our null parcel-wise and significant vertex-wise results provide some support for this view. This may also explain why, historically, the methods with the highest spatial resolution were those that provided the most convincing evidence for illusory contour formation in V1 and V2 (Grosof et al., 1993; e.g., Lee and Nguyen, 2001; Kok and de Lange, 2014). Higher resolution fMRI or more salient contours (Seghier et al., 2000) may be needed to bring out effects more fully within V1 and V2.

Frontoparietal cortex and high-level feedback to mid-level vision

Frontoparietal network regions were differentially active in orbitofrontal, dorsolateral prefrontal, and posterior parietal cortex. Although frontoparietal regions could not be used to infer activity in secondary visual network regions in our ActFlow analyses, they were directly connected to dorsal attention network regions, which themselves could predict activity within this visual network.

Frontoparietal involvement has been at least indirectly suggested by prior work. For example, cognitively biasing observers to see edge elements as disconnected worsened the discrimination of illusory but not fragmented shapes (Keane et al., 2012). A rapid and dramatic insight learning has been shown to occur within the first dozen trials of the “fat/thin” task, suggesting that properly seeing an illusory shape requires deploying an appropriate decisional template (Rubin et al., 1997; see also, Gold and Shubel, 2006). As noted in the Introduction, peak orbitofrontal modulation from passively-viewed Kanizsa shapes arose 340 ms post stimulus onset (Halgren et al., 2003). In eight month- (but not six month-) old infants, gamma

band oscillations (40 HZ) from Kanizsa shapes were generated over frontal electrodes between 240-320 ms (Csibra et al., 2000).

Frontoparietal cortex may serve to generate expectation-based predictions that can either help observers notice less salient illusory contours (Keane et al., 2012 p.416), or recover object structure when interpolated contours are absent (when edge elements are extremely sparse, misaligned, or misoriented (Wyatte et al., 2014; Keane, 2018). For example, highly degraded line drawings (Sehatpour et al., 2006) and so-called salient regions (which lack illusory contours but which induce the formation of a blurry lightened/darkened surface, Stanley and Rubin, 2003) may activate lateral occipital regions at later stages of processing (Shpaner et al., 2009), which could reflect the brain's best guesses about the precise shape of the incoming stimulus.

It is important to note that high-level feedback of the type described is compatible with an automatic illusory contour formation process (Keane, 2018). Behavioral and electrophysiological studies have shown that illusory contours maximally form within ~120 ms (Lee and Nguyen, 2001; Murray et al., 2002; Guttman and Kellman, 2004), which is well before the arrival of higher-order feedback. Higher-order cortical feedback may be ineffectual even after its arrival, if it must compete with persistingly salient bottom-up signals (Desimone and Duncan, 1995; McMains and Kastner, 2010; Keane, 2018). Thus, frontoparietal signals may primarily be important for noticing/using illusory contours for shape recognition tasks or for cognitively inferring the existence of contours when the stimulus conditions prevent salient illusory contours.

A sketch of activity flow during visual shape completion and a possible role for the dorsal attentional network as a relay between frontoparietal cortex and mid-level vision

Brain activity flow mapping with fMRI lacks the temporal resolution and directionality to fully characterize how task regions interact during visual shape completion. However, our results, combined with others, contribute to an emerging picture. In the initial afferent volley, activity likely flows from early visual areas, to mid-level shape areas such as V4 and lateral occipital complex (Wokke et al., 2013) and then back down to V2 and then V1 via an automatic, local recurrent circuit (Lee and Nguyen, 2001; Shpaner et al., 2013; Wyatte et al., 2014). As the illusory contours are constructed within the first ~150 ms (Guttman and Kellman,

2004), the mid-level visual areas—including area PH—simultaneously relay information forward to posterior parietal regions and then to orbitofrontal and dorsolateral prefrontal cortices (Cavada and Goldman-Rakic, 1989). Finally, information flows back down the cortical hierarchy via the same route or even directly back to the secondary visual areas (Bar, 2003; Halgren et al., 2003). In the later stages of shape completion, the anterior cingulate cortex, dorsolateral prefrontal cortex, inferior frontal junction, and intraparietal sulcus (e.g., a24, IFSa, p9-46v, IFJp, IP0, IP1) may also jointly segregate and sustain illusory-contour-defined shape representations (Naughtin et al., 2016; 2018). This sketch is obviously far from complete but provides a scaffold upon which to build more sophisticated models.

Objections, limitations, and opportunities for future research

Although all subjects were repeatedly instructed to centrally fixate, eye movement confounds cannot be completely ruled out. However, even if we were to discover task-related eye movement differences and even if these differences could be linked to differential brain activity (e.g., in LIPd), the result in itself would be difficult to interpret. It could imply that shape perception generates different fixation patterns or the other way around. An independent study would be needed to tease the two apart, which is beyond the scope of the present investigation.

Past psychophysical studies have shown similar illusory and fragmented task performance (Keane et al., 2014) but in the present study the fragmented task was about 6 percent better. Why? A possible reason is that past studies had a verbal response and ours had a button press. The congruence between the left and right rotations and left and right button press may have conferred a small but consistent benefit perhaps by diminishing the likelihood of misremembering the mapping between keypress and response. We do not view this as problematic, since the effects arose when the congruence benefit was behaviorally eliminated—both in RT and accuracy. Therefore, while large task accuracy differences clearly alter the neural data (as in the easy versus hard contrast), smaller differences appear to have little effect.

Limitations are worth noting. We have confined our results to cortex but recent network partitions have been extended to include 358 subcortical structures (Ji et al., 2019). Exploring these regions would require much larger subject samples to adequately correct for multiple

comparisons, but would likely yield new insights. Another limitation is that even though our shape completion study was more sensitive than most previous ones, a larger sample and a higher field magnet will likely reveal additional regions, connections, and networks. Finally, as has already been noted, the slow hemodynamic response prevents a full description of the temporal dynamics.

Notwithstanding the foregoing, the present research leverages a brain activity mapping method and recent advances in functional MRI to demonstrate the likely relevance of dorsal attention connections for visual shape completion. The secondary visual network plays a dominant role in the process, but portions of at least four other networks—including the frontoparietal—participate in a densely interconnected network coalition, which can be used to model activations related to shape completion. A logical next step will be to apply neurostimulation to probe parcel-wise causal interactions or electrophysiology to assess their activity flow dynamics.

References

Anticevic A, Cole MW, Murray JD, Corlett PR, Wang X-J, Krystal JH (2012) The role of default network deactivation in cognition and disease. Trends Cogn Sci (Regul Ed) 16:584–592.

Bar M (2003) A cortical mechanism for triggering top-down facilitation in visual object recognition. J Cogn Neurosci 15:600–609.

Benjamini Y, Hochberg J (1995) Controlling the false discovery rate: A practical and powerful approach to multiple testing. Journal of the Royal Statistical Society Series B-Methodological 57:289–300.

Cavada C, Goldman-Rakic PS (1989) Posterior parietal cortex in rhesus monkey: II. Evidence for segregated corticocortical networks linking sensory and limbic areas with the frontal lobe. J Comp Neurol 287:422–445.

Ciric R, Wolf DH, Power JD, Roalf DR, Baum GL, Ruparel K, Shinohara RT, Elliott MA, Eickhoff SB, Davatzikos C, Gur RC, Gur RE, Bassett DS, Satterthwaite TD (2017) Benchmarking of participant-level confound regression strategies for the control of motion artifact in studies of functional connectivity. Neuroimage 154:174–187.

Cole MW, Bassett DS, Power JD, Braver TS, Petersen SE (2014) Intrinsic and task-evoked network architectures of the human brain. Neuron 83:238–251.

Cole MW, Ito T, Bassett DS, Schultz DH (2016) Activity flow over resting-state networks shapes cognitive task activations. Nature Neuroscience 19:1718–1726.

Cox MA, Schmid MC, Peters AJ, Saunders RC, Leopold DA, Maier A (2013) Receptive field focus of visual area V4 neurons determines responses to illusory surfaces. Proc Natl Acad Sci USA 110:17095–17100.

Csibra G, Davis G, Spratling MW, Johnson MH (2000) Gamma oscillations and object processing in the infant brain. Science 290:1582–1585.

Desimone R, Duncan J (1995) Neural mechanisms of selective visual attention. Annu Rev Neurosci 18:193–222.

Esteban O, Birman D, Schaer M, Koyejo OO, Poldrack RA, Gorgolewski KJ (2017) MRIQC: Advancing the automatic prediction of image quality in MRI from unseen sites Bernhardt BC, ed. PLOS ONE 12:e0184661.

Glasser MF, Coalson TS, Robinson EC, Hacker CD, Harwell J, Yacoub E, Uğurbil K, Andersson J, Beckmann CF, Jenkinson M, Smith SM, Van Essen DC (2016) A multi-modal parcellation of human cerebral cortex. Nature 536:171–178.

Glasser MF, Sotiropoulos SN, Wilson JA, Coalson TS, Fischl B, Andersson JL, Xu J, Jbabdi S, Webster M, Polimeni JR, Van Essen DC, Jenkinson M, Consortium FTW-MH (2013) The

minimal preprocessing pipelines for the Human Connectome Project. Neuroimage 80:105–124.

Gold JM, Murray RF, Bennett PJ, Sekuler AB (2000) Deriving behavioural receptive fields for visually completed contours. Current Biology 10:663–666.

Gold JM, Shubel E (2006) The spatiotemporal properties of visual completion measured by response classification. Journal of Vision 6:356–365.

Grosof DH, Shapley RM, Hawken MJ (1993) Macaque V1 neurons can signal “illusory” contours. Nature 365:550–552.

Grzeczkowski L, Clarke AM, Francis G, Mast FW, Herzog MH (2017) About individual differences in vision. Vision Research 141:282–292.

Guttman SE, Kellman PJ (2004) Contour interpolation revealed by a dot localization paradigm. Vision Research 44:1799–1815.

Halgren E, Mendola J, Chong CDR, Dale AM (2003) Cortical activation to illusory shapes as measured with magnetoencephalography. Neuroimage 18:1001–1009.

Haynes J-D (2015) A Primer on Pattern-Based Approaches to fMRI: Principles, Pitfalls, and Perspectives. Neuron 87:257–270.

Henrich J, Heine SJ, Norenzayan A (2010) The weirdest people in the world? Behav Brain Sci 33:61–83.

Huxlin KR, Saunders RC, Marchionini D, Pham HA, Merigan WH (2000) Perceptual deficits after lesions of inferotemporal cortex in macaques. Cereb Cortex 10:671–683.

Iacaruso MF, Gasler IT, Hofer SB (2017) Synaptic organization of visual space in primary visual cortex. Nature 547:449–452.

Ji JL, Spronk M, Kulkarni K, Repovs G, Anticevic A, Cole MW (2019) Mapping the human brain's cortical-subcortical functional network organization. Neuroimage 185:35–57.

Keane BP (2018) Contour interpolation: A case study in Modularity of Mind. Cognition 174:1–18.

Keane BP, Joseph J, Silverstein SM (2014) Late, not early, stages of Kanizsa shape perception are compromised in schizophrenia. Neuropsychologia 56:302–311.

Keane BP, Lu H, Kellman PJ (2007) Classification images reveal spatiotemporal contour interpolation. Vision Research 47:3460–3475.

Keane BP, Lu H, Papathomas TV, Silverstein SM, Kellman PJ (2012) Is interpolation cognitively encapsulated? Measuring the effects of belief on Kanizsa shape discrimination and illusory contour formation. Cognition 123:404–418.

Keane BP, Paterno D, Kastner S, Krekelberg B, Silverstein SM (2019) Intact illusory contour formation but equivalently impaired visual shape completion in first- and later-episode schizophrenia. J Abnorm Psychol 128:57–68.

Kellman PJ, Shipley T (1991) A theory of visual interpolation in object perception. Cogn Psychol 23:141.

Kok P, de Lange FP (2014) Shape Perception Simultaneously Up- and Downregulates Neural Activity in the Primary Visual Cortex. Current Biology 24:1531–1535.

Krienen FM, Yeo BTT, Buckner RL (2014) Reconfigurable task-dependent functional coupling modes cluster around a core functional architecture. Philosophical Transactions of the Royal Society B: Biological Sciences 369:20130526.

Kruggel F, Herrmann CS, Wiggins CJ, Cramon von DY (2001) Hemodynamic and Electroencephalographic Responses to Illusory Figures: Recording of the Evoked Potentials during Functional MRI. Neuroimage 14:1327–1336.

Larsson J, Amunts K, Gulyás B, Malikovic A, Zilles K, Roland PE (1999a) Neuronal correlates of real and illusory contour perception: functional anatomy with PET. Eur J Neurosci 11:4024–4036.

Larsson J, Amunts K, Gulyás B, Malikovic A, Zilles K, Roland PE (1999b) Neuronal correlates of real and illusory contour perception: functional anatomy with PET. Eur J Neurosci 11:4024–4036.

Lee T, Nguyen M (2001) Dynamics of subjective contour formation in the early visual cortex. Proceedings of the National Academy of Sciences 98:1907–1911.

Malikovic A, Amunts K, Schleicher A, Mohlberg H, Kujovic M, Palomero-Gallagher N, Eickhoff SB, Zilles K (2016) Cytoarchitecture of the human lateral occipital cortex: mapping of two extrastriate areas hOc4la and hOc4lp. Brain Struct Funct 221:1877–1897.

McMains SA, Kastner S (2010) Defining the units of competition: influences of perceptual organization on competitive interactions in human visual cortex. J Cogn Neurosci 22:2417–2426.

Mill RD, Gordon BA, Balota DA, Cole MW (2020) Predicting dysfunctional age-related task activations from resting-state network alterations. Neuroimage:117167–37.

Mur M, Bandettini PA, Kriegeskorte N (2009) Revealing representational content with pattern-information fMRI--an introductory guide. Soc Cogn Affect Neurosci 4:101–109.

Murray M, Wylie G, Higgins B, Javitt D, Schroeder C, Foxe J (2002) The spatiotemporal dynamics of illusory contour processing: combined high-density electrical mapping, source analysis, and functional magnetic resonance imaging. Journal of Neuroscience 22:5055.

Murray MM, Imber ML, Javitt DC, Foxe JJ (2006) Boundary Completion Is Automatic and Dissociable from Shape Discrimination. Journal of Neuroscience 26:12043–12054.

Naughtin CK, Mattingley JB, Bender AD, Dux PE (2018) Decoding early and late cortical contributions to individuation of attended and unattended objects. CORTEX 99:45–54.

Naughtin CK, Mattingley JB, Dux PE (2016) Distributed and Overlapping Neural Substrates for Object Individuation and Identification in Visual Short-Term Memory. Cerebral Cortex 26:566–575.

Orban GA, Van Essen D, Vanduffel W (2004) Comparative mapping of higher visual areas in monkeys and humans. Trends Cogn Sci (Regul Ed) 8:315–324.

Peirce JW (2007) PsychoPy—Psychophysics software in Python. J Neurosci Methods 162:8–13.

Pelli DG (1997) The VideoToolbox software for visual psychophysics: transforming numbers into movies. Spat Vis 10:437–442.

Pillow J, Rubin N (2002) Perceptual completion across the vertical meridian and the role of early visual cortex. Neuron 33:805–813.

Power JD, Barnes KA, Snyder AZ, Schlaggar BL, Petersen SE (2012) Spurious but systematic correlations in functional connectivity MRI networks arise from subject motion. Neuroimage 59:2142–2154.

Power JD, Cohen AL, Nelson SM, Wig GS, Barnes KA, Church JA, Vogel AC, Laumann TO, Miezin FM, Schlaggar BL, Petersen SE (2011) Functional Network Organization of the Human Brain. Neuron 72:665–678.

Ringach D, Shapley R (1996) Spatial and temporal properties of illusory contours and amodal boundary completion. Vision Research 36:3037–3050.

Rubin N, Nakayama K, Shapley R (1997) Abrupt learning and retinal size specificity in illusory-contour perception. Curr Biol 7:461–467.

Sáry G, Köteles K, Kaposvári P, Lenti L, Csifcsák G, Frankó E, Benedek G, Tompa T (2008) The representation of Kanizsa illusory contours in the monkey inferior temporal cortex. European Journal of Neuroscience 28:2137–2146.

Schultz DH, Ito T, Solomyak LI, Chen RH, Mill RD, Anticevic A, Cole MW (2018) Global connectivity of the fronto-parietal cognitive control network is related to depression symptoms in the general population. Netw Neurosci 3:107–123.

Seghier M, Dojat M, Delon-Martin C, Rubin C, Warnking J, Segebarth C, Bullier J (2000) Moving illusory contours activate primary visual cortex: an fMRI study. Cereb Cortex 10:663–670.

Seghier ML, Vuilleumier P (2006) Functional neuroimaging findings on the human perception of illusory contours. Neurosci Biobehav Rev 30:595–612.

Sehatpour P, Molholm S, Javitt DC, Foxe JJ (2006) Spatiotemporal dynamics of human object recognition processing: An integrated high-density electrical mapping and functional imaging study of “closure” processes. Neuroimage 29:605–618.

Shpaner M, Molholm S, Forde E, Foxe JJ (2013) Disambiguating the roles of area V1 and the lateral occipital complex (LOC) in contour integration. Neuroimage 69:146–156.

Shpaner M, Murray MM, Foxe JJ (2009) Early processing in the human lateral occipital complex is highly responsive to illusory contours but not to salient regions. European Journal of Neuroscience 30:2018–2028.

Spronk M, Kulkarni K, Ji JL, Keane BP, Anticevic A, Cole MW (2018) A whole-brain and cross-diagnostic perspective on functional brain network dysfunction. BioRxiv:1–23.

Stanley DA, Rubin N (2003) fMRI activation in response to illusory contours and salient regions in the human lateral occipital complex. Neuron 37:323–331.

Stark DE, Margulies DS, Shehzad ZE, Reiss P, Kelly AMC, Uddin LQ, Gee DG, Roy AK, Banich MT, Castellanos FX, Milham MP (2008) Regional variation in interhemispheric coordination of intrinsic hemodynamic fluctuations. Journal of Neuroscience 28:13754–13764.

Wokke ME, Vandenbroucke ARE, Scholte HS, Lamme VAF (2013) Confuse your illusion: feedback to early visual cortex contributes to perceptual completion. Psychological Science 24:63–71.

Wyatte D, Jilk DJ, O'Reilly RC (2014) Early recurrent feedback facilitates visual object recognition under challenging conditions. Front Psychol 5:760–10.